AMERICAN
METEOROLOGICAL
SOCIETY

Bulletin of the American Meteorological Society

The DOI for this manuscript is doi: 10.1175/BAMS-D-13-00238.1

Cloud Banding and Winds in Intense European Cyclones: Results from the DIAMET Project

G. Vaughan[1], J. Methven[4], D. Anderson[11], B. Antonescu[2] , L. Baker[4], T. P. Baker[7], S. P. Ballard[9], K. N. Bower[2], P. R. A. Brown[10], J. Chagnon[3], T. W. Choularton[2], J. Chylik[8], P. J. Connolly[2], P. A. Cook[8], R. J. Cotton[10] , J. Crosier[1], C. Dearden[2], J. R. Dorsey[1], T. H. A. Frame[3], M. W. Gallagher[2], M. Goodliff[4], S. L. Gray[4], B. J. Harvey[4], P. Knippertz[12], H. W. Lean[9], D. Li[9], G. Lloyd[2], O. Martínez –Alvarado[4], J. Nicol[3], J. Norris[2], E. Öström[10], J. Owen[7], D. J. Parker[7], R. S. Plant[4], I. A. Renfrew[8], N. M. Roberts[9], P. Rosenberg[7], A. C. Rudd[4], D. M. Schultz[2], J. P.Taylor[10], T. Trzeciak[7], R. Tubbs[9], A. K. Vance[10], P. J. van Leeuwen[5], A. Wellpott[11], A. Woolley[11]

AFFILIATIONS:

[1] National Centre for Atmospheric Science (NCAS) , University of Manchester, Manchester, UK

[2] Centre for Atmospheric Science, University of Manchester, Manchester, UK

[3] NCAS, University of Reading, Reading, UK

[4] Department of Meteorology, University of Reading, Reading, UK

[5] National Centre for Earth Observation (NCEO), University of Reading, Reading, UK

[6] NCAS, University of Leeds, Leeds, UK

[7] School of Earth and Environment,University of Leeds, Leeds, UK

[8] School of Environmental Science, University of East Anglia, Norwich, UK

[9] Met Office, University of Reading, Reading, UK

[10] Met Office, Exeter, UK

[11] Facility for Airborne Atmospheric Measurement, Cranfield, UK

[12] Institute for Meteorology and Climate Research, Karlsruhe Institute of Technology, Germany

[1]Corresponding address: SEAES, Simon Building, Oxford Rd, Manchester, M13 9PL, UK

Abstract

The DIAMET (DIAbatic influences on Mesoscale structures in ExTratropical storms) project aims to improve forecasts of high-impact weather in extratropical cyclones through field measurements, high-resolution numerical modeling, and improved design of ensemble forecasting and data assimilation systems. This article introduces DIAMET and presents some of the first results. Four field campaigns were conducted by the project, one of which, in late 2011, coincided with an exceptionally stormy period marked by an unusually strong, zonal North Atlantic jet stream and a succession of severe windstorms in northwest Europe. As a result, December 2011 had the highest monthly North Atlantic Oscillation index (2.52) of any December in the last 60 years. Detailed observations of several of these storms were gathered using the UK's BAe146 research aircraft and extensive ground-based measurements. As an example of the results obtained during the campaign, observations are presented of cyclone Friedhelm on 8 December 2011, when surface winds with gusts exceeding 30 m s^{-1} crossed central Scotland, leading to widespread disruption to transportation and electricity supply. Friedhelm deepened 44 hPa in 24 hours and developed a pronounced bent-back front wrapping around the storm center. The strongest winds at 850 hPa and the surface occurred in the southern quadrant of the storm, and detailed measurements showed these to be most intense in clear air between bands of showers. High-resolution ensemble forecasts from the Met Office showed similar features, with the strongest winds aligned in linear swaths between the bands, suggesting that there is potential for improved skill in forecasts of damaging winds.

Capsule: New aircraft measurements, together with high-resolution modeling, reveal fine-scale wind structure in an intense extratropical windstorm.

Extratropical cyclones approaching western Europe along the North Atlantic storm track are a major cause of damaging winds and heavy precipitation. A particular problem in forecasting these cyclones is that the highest-impact weather within them arises from mesoscale structures such as fronts and bands of strong winds. These structures are influenced by diabatic processes (those which add or remove heat from the air) such as latent heating and cooling associated with phase changes of water, fluxes of heat and moisture from the Earth's surface, and radiative flux convergence. Key elements in diabatic processes are turbulence, convection and cloud physics – small-scale phenomena which cannot be represented explicitly in numerical weather prediction models. They must therefore be parameterised, introducing a source of systematic uncertainty in the models. Detailed observations of real events are needed to test the models and ultimately to improve the parameterisation of small-scale processes.

Here we report on initial results from the DIAMET (DIAbatic influences on Mesoscale structures in ExTratropical storms) project, which aims to improve our understanding and predictions of mesoscale structures within extratropical cyclones by means of field measurements, high-resolution modeling and improved design of ensemble forecasting and data assimilation systems. The modeling component of the project includes evaluation of the Met Office high-resolution ensemble forecasts, the probability forecasts of mesoscale structures, the stochastic physics scheme used in the ensemble, and the ability of the model to represent the structures that bring high-impact weather. This paper provides an overall introduction to DIAMET with particular emphasis on the field measurements and the way these are used to test and improve models.

The winter campaign of DIAMET was conducted during a period of particularly intense storm activity over the North Atlantic. As an example of an intense storm, and to illustrate the scientific approach used in DIAMET, we present a more detailed study of Cyclone Friedhelm on 8 December

2011. The strongest low-level winds in this storm occurred on its southern and southwestern flanks. We concentrate in this paper on the prominent cloud banding often found in the southern quadrant of intense storms (Neiman et al. 1993; Grønås 1995; Browning and Field 2004), where our observations reveal a relation between the wind strength and the cloud bands. We show that a similar relation appears in an experimental trial of the Met Office high-resolution ensemble forecast system.

THE DIAMET PROJECT. The DIAMET project is one of the three components of the UK Natural Environment Research Council's Storm Risk Mitigation Programme (http://www.bgs.ac.uk/stormrm/home.html), and is a collaboration between British academic groups and the Met Office. The main elements of the project, together with results published so far, can be summarised as:

a) Use of field measurements and detailed numerical modelling to improve understanding of key processes (Chagnon et al. 2013, Martínez-Alvarado et al. 2014, Norris et al. 2014)

b) Critical assessments of the performance of parameterisations of convection (Martínez-Alvarado and Plant 2013), air-sea fluxes (Cook and Renfrew 2014) and microphysics (Dearden et al. 2014, Lloyd et al. 2014) in numerical weather prediction models and

c) Addressing fundamental aspects of predictability using ensembles, and improving data assimilation methods for better short-term forecasting (Baker et al. 2014)

The scientific approach of DIAMET concentrates on the effect of diabatic processes on the distribution of potential vorticity (PV) and its consequences for the evolution of weather systems. PV combines the vertical stability of the atmosphere with the horizontal shear and rotation of the wind field, and is materially conserved in the absence of diabatic and frictional processes. It is a local measure of circulation about a point and its distribution is fundamental to our understanding

of Rossby waves and the evolution of cyclones (e.g. Hoskins et al. 1985). Cyclone development typically arises through interaction between a Rossby wave on the tropopause and large-scale horizontal waves in temperature near the ground, with the surface cyclone center positioned to the east of the upper-level PV maximum (trough). This process is well understood, but the effects of PV anomalies produced by diabatic processes are much less clear. It is possible to attribute diabatically-generated PV anomalies to the processes that produce them in a forecast model (e.g., Chagnon et al. 2013), but these diagnostics need to be tested by comparison with observations. A main goal of DIAMET is to use detailed measurements of dynamics, cloud physics and air-sea fluxes to calculate diabatic heating rates in cyclones and thereby evaluate how well the diabatic production and removal of PV anomalies are represented in models. Key scientific questions are:

a) How do latent heating and air-sea fluxes modify the mesoscale potential vorticity distribution in an extratropical cyclone?
b) How do such modifications affect the precipitation and wind fields and therefore the impact of the cyclone on society?
c) Do these modifications affect the overall development of the cyclone (and others downstream) or are they only important locally?
d) How sensitive are numerical forecasts to the parameterisation of latent heating and air-sea fluxes? Can model error from these sources be quantified?

From September 2011 to August 2012, DIAMET conducted four field campaigns lasting several weeks each to examine cyclones around the UK and Ireland. The primary measurement platform was the BAe146 aircraft of the UK's Facility for Airborne Atmospheric Measurements (FAAM, http://www.faam.ac.uk/) carrying instrumentation to measure winds, thermodynamic parameters, microphysics and chemical tracers. A summary of the relevant instrumentation for DIAMET is shown in Table 1. The FAAM aircraft can operate up to an altitude of 10 km with an

endurance of around 5 hours (see Renfrew et al. 2008 for more details and flight examples). In several DIAMET cases, double flights were conducted, with a break for refuelling mid-mission. For three of the four campaigns, the aircraft was based in Cranfield, north of London, but in the winter campaign of November–December 2011 it was based at Exeter, near to the Met Office headquarters (see Fig. 5 for locations described in the text). Ground-based measurements were also a crucial part of DIAMET: 3D precipitation-radar measurements from the Chilbolton Facility for Atmospheric and Radio Research (Browning et al. 2007); precipitation maps from the Met Office's operational precipitation-radar network (Harrison et al. 2009); continuous measurements from wind profilers, especially the UK Mesosphere–Stratosphere–Troposphere VHF profiler at Aberystwyth in Wales (Vaughan 2002); and surface data from the Met Office's network of around 270 automatic weather stations (AWS). Fifty-five additional radiosonde launches were made from selected stations on intensive observation period (IOP) days.

There were fifteen flying days (Table 2) covering fourteen DIAMET IOPs (flights into the same meteorological system on successive days are grouped into the same IOP). Nine of these IOPs were in 2011 and five in 2012, and all but one involved the FAAM aircraft. The exception, IOP 10, was declared a DIAMET IOP because of the passage of a mesoscale convective system over the Chilbolton radar which led to widespread flooding in the Severn valley, the largest river catchment in the UK. Three flights are also listed from the T-NAWDEX (THORPEX-North Atlantic Waveguide and Downstream impact Experiment) Pilot campaign in November 2009. They were conducted by the DIAMET team as a preliminary investigation, and have been analysed as part of the DIAMET project (labelled TNP1-3 in Table 2).

148 **THE NORTH ATLANTIC WEATHER REGIME OF EARLY WINTER 2011–2012.** The second DIAMET aircraft campaign (24 November to 14 December 2011) was characterized by an unusually strong
150 zonal jet stream across the North Atlantic and a rapid succession of intense cyclones, many of which crossed northwest Europe. One way to characterize the large-scale weather pattern over
152 the North Atlantic is to examine the North Atlantic Oscillation (NAO) index, a normalized measure of the pressure difference between Iceland and the Azores. Positive values of the NAO are
154 associated with stormy weather over northwest Europe, with milder temperatures and greater precipitation than the negative phase. Daily NAO index values are provided by the
156 NOAA/NCEP/Climate Prediction Center for January 1950 to June 2012 (http://www.cpc.ncep.noaa.gov/products/precip/CWlink/pna/nao.shtml). Remarkably, 30
158 November, 3 December, and 6 December 2011—all within the DIAMET campaign period—appear in the top 0.4% of daily values of this long time series (22,825 days). December 2011 had the
160 highest monthly NAO index (2.52) of any December and the third highest for all months of the entire time series.

162 The zonal wind strength between 1 November 2011 and 31 January 2012 is shown in Fig. 1a together with the climatological mean and standard deviation for this time of year. The statistics
164 are calculated from the average of zonal wind at 300 hPa across the North Atlantic (between 40-60^{o}N and 10-60^{o}W) obtained from 6-hourly ERA-Interim re-analysis data (Dee et al. 2011). The
166 climatology was obtained from the entire ERA-Interim dataset 1979–2010 by calculating the mean and standard deviation of each calendar date across all years and then smoothing the resulting
168 series with a 7-day running mean. The zonal wind was exceptionally strong during the DIAMET campaign with values more than one standard deviation above the climatological mean for most
170 of the period and more than two standard deviations for a few days. Comparing the histogram of North Atlantic zonal wind compiled from data during the 21 days of the DIAMET campaign with

172 that during the three-month period November 2011 – January 2012 (Fig. 1b), and the corresponding histogram from all Nov-Dec-Jan periods in the ERA-Interim dataset, further
174 underlines the anomalous conditions during this period.

Between 22 November and 10 January, the Free University of Berlin named 29 significant cyclones
176 affecting Europe as part of their Adopt-A-Vortex scheme, corresponding to one new storm forming every 1.7 days. All but one of these storms passed over or near the UK or affected the UK
178 with their frontal systems. Many of the stronger storms are reflected by *decreases* in the average zonal wind across the North Atlantic. These decreases occur as the Rossby waves at tropopause
180 level reach large amplitude and break, causing the jet stream to split, with weaker average flow in the 40–60°N band. Decreases in jet stream strength (often leading to minima) were associated
182 with the intense cyclonic storms:

- Zafer (1 December, DIAMET IOP6) was a small-scale intense low north of Scotland.
184 • Friedhelm (7–8 December, IOP8) was the explosively deepening cyclone discussed in Section 4.
- Hergen (12-13 December, IOP9) passed north of Scotland extending an active warm front
186 across the UK.
- Joachim (15–16 December) was fast moving and tracked directly into central Europe causing
188 widespread gales and heavy rain associated with some damage in southern Germany.
- Patrick (25 December) and Robert (28 December) followed similar tracks across northern
190 Scotland.
- Ulli and Andrea (3–5 January) again brought high winds to Scotland and northern England.

192 In contrast, the dips to relatively low values on 18–19 December 2011 and around 12 January 2012 were associated with ridge-building not linked to a preceding cyclone.

194

We now present a more detailed study of cyclone Friedhelm, the subject of DIAMET IOP8.

196

DIAMET IOP8 – FLIGHT INTO THE CENTER OF CYCLONE FRIEDHELM. The passage of extratropical
198 cyclone Friedhelm resulted in considerable disruption to transport and some damage to infrastructure over the central belt of Scotland. Friedhelm started as a shallow wave on a trailing
200 cold front over Newfoundland at 1200 UTC on 6 December 2011. As it crossed the Atlantic, the storm crossed the axis of the polar jet stream and deepened spectacularly—44 hPa between mid-
202 day on 7 December and mid-day on the 8th, easily qualifying as a meteorological bomb (Sanders and Gyakum 1980). Structurally, Friedhelm resembled a Shapiro-Keyser cyclone (Shapiro and
204 Keyser 1990) with a frontal fracture (weakening of the northern part of the cold front near the warm front) followed by wrapping of cold air at low levels around the northern flank of a warmer
206 cyclone center. By the time Friedhelm reached western Scotland early on 8 December, the storm was in its mature stage with a central pressure of 957 hPa (Fig. 2). A large separation between the
208 warm sector and the cyclone center showed that the cyclone had occluded (Schultz and Vaughan 2011), with a bent-back front corresponding to the mass of cloud curling westward around
210 Scotland (Fig. 3a). Southwest of the cyclone center, bands of low cloud extended eastwards towards Scotland from beneath the mid-level cloud deck. Corresponding banding was observed in
212 light precipitation over the sea to the west of Scotland by the Met Office radar network (Fig. 3b). These bands (labelled A–D) moved east-southeastward across central Scotland. The storm
214 continued to move eastward towards Scandinavia, with the strongest winds crossing to the east side of Scotland by early evening. The precipitation bands crossed Scotland with the storm and
216 were especially prominent around 1800 UTC over central Scotland (Fig. 4a). The cyclone also wrapped up further with the strongest winds moving into the southern and then southeastern
218 side of the low pressure center.

Figure 4b shows the maximum wind gusts measured on 10-m masts at selected AWS across the
220 northern UK during 8 December. The numbers are coloured by the time of maximum gust to illustrate the eastward progression of the high winds associated with the storm. Maxima of
222 around 30 m s^{-1} (67 mph) occur over a wide area of Scotland, notably in the highly populated region between Glasgow and Edinburgh. The previous day the Met Office had issued its first ever
224 red alert for winds (warning the public to take action), allowing precautions to be taken including the closure of schools, roads and bridges in the threatened areas. Over some of the Scottish
226 mountains, much higher winds were recorded – the highest being 74 m s^{-1} (165 mph) reported on the summit of Cairn Gorm (1237 m), around 100 km north-northwest of Leuchars.

228 The FAAM aircraft was tasked on this day with investigating the region of strongest winds to the south and southwest of the cyclone center. Such winds are often associated with a *cold conveyor*
230 *belt*, a low-level airstream which wraps around a cyclone as it develops (Carlson 1980). In addition, some Shapiro-Keyser cyclones develop *sting jets* – cores of very strong low-level winds associated
232 with descending airstreams ahead of the mid-level cloud head (Browning 2004; Clark et al. 2005). Indeed, evidence for such features during the passage of Cyclone Ulli on 3 January 2012 was
234 presented by Smart and Browning (2013). There have been other aircraft flights through intense extratropical cyclones; for example, Neiman and Shapiro (1993) and Neiman *et al* (1993)
236 presented observations of an extremely rapidly developing cyclone (ERICA IOP4) which had similar bent-back frontal structure to Friedhelm and prominent rainbands in the same sector of the storm
238 (their Fig. 19). DIAMET was able to build on these results by measuring the wind structure associated with precipitation bands together with their cloud microphysical properties.
240 The aircraft took off at 1048 UTC from Exeter, timed to intercept the cyclone center before it had traversed Scotland. Baker et al. (2013) described the thrill of the flight and showed photographs
242 taken from within the cyclone center looking across the curving cloud bands, as well as the sea

state in the high-wind region. The first leg of the flight, at an altitude of 7 km, launched ten
244 dropsondes along the west coast of Scotland to measure the thermodynamic and wind structure
along a transect through the storm to the north of the cold front and reached the cyclone center
246 at 1234 UTC (Fig. 5).

248 Figure 6 shows relative humidity with respect to ice (RHi), potential temperature and horizontal
winds along the dropsonde section. The sloping temperature gradient, between 2 and 6 km in the
250 southern part of the section, separated dry air above it from the moister air below (northwest of
the cold front). The wind-speed cross section shows the upper-level jet stream between 54° and
252 55.5°N, exceeding 60 m s^{-1} at 6-km altitude above a layer of pronounced wind shear.

A second, weaker, temperature gradient is shown below 4 km, north of 57°N. Here, temperature
254 increased with latitude (Fig. 6), associated with the bent-back warm front which had wrapped
around to the south side of the cyclone. The pool of warmer air at low levels near the core of this
256 kind of cyclone is called a seclusion (Shapiro and Keyser 1990). The low-level wind maximum that
was the focus of this mission lay on the southern flank of this front. An L-shaped wind maximum
258 extended from 4 km down to 1.5 km at 56.3°N, with an extension northward to 57.1°N below 2.5
km; a low-level zonal-wind maximum is expected from approximate thermal wind balance with
260 the poleward increase in potential temperature. Martínez-Alvarado et al. (2014) found that the air
entering the strong wind region south of Friedhelm's center comprised three airstreams with
262 distinct trajectory origins and observed tracer composition. Two airstreams were associated with
the cold conveyor belt – the air was cloudy and back-trajectories stayed at low levels wrapping
264 around the cyclone core – whereas the third resembled a sting jet which left the tip of the cloud
head to the west of the cyclone and descended towards the east-southeast. In Fig. 6, the strongest
266 winds, measured by sondes 5–7, coincided with relative humidity values exceeding 80% beneath

the sloping isentropes, suggesting that the cold conveyor belt dominated the low-level winds along this section.

After executing the second dropsonde section to the southwest of the cyclone center (Fig. 5; see Martínez-Alvarado et al. 2014 for cross-section), the aircraft descended to make *in-situ* measurements at lower altitudes. Of particular interest for this paper are the low-level legs to the west of Scotland at around 1500 UTC, through the region of strongest low-level winds, which are discussed in the next section. Further low-level work was conducted after refuelling in Teesside, by which time the strongest winds were located to the east of Scotland. Here the relative humidity (with respect to ice) of the fastest-moving air was around 42%, suggesting descent of around 150 hPa from initial saturation. Turbulent mixing was intense at low levels on this flight – the turbulent kinetic energy, calculated from the 32-Hz turbulence probe, was 7–10 $m^2 s^{-2}$ – and the aircraft became coated in sea salt even when flying at 500 m above sea level. (Observations of turbulence throughout the DIAMET experiment are reported in Cook and Renfrew 2014.) On this boundary-layer leg (lasting 30 minutes), the gradient in potential temperature was almost uniform with values decreasing towards the south, whereas wind speed increased to an average of 47 m s^{-1} at the southern end (not shown). Therefore, the aircraft was able to make detailed measurements of the wind field and thermodynamic variables in the region of maximum wind speed to the south of the cyclone center, both west and east of Scotland.

BANDING IN CLOUD, PRECIPITATION, AND WINDS ON THE SOUTHERN FLANK OF FRIEDHELM.

We now turn to the question of how the cloud and precipitation bands (Fig. 3) were linked to the severe surface winds (Fig. 4b), concentrating on the low-level legs measured around 1500 UTC as the aircraft flew from Islay northwards towards Tiree in a region of banded precipitation within the cold conveyor belt airstream of the cyclone (Fig. 7). The bands in Fig. 7 are numbered from south to north and fall in two groups: the northern group (B) intersected by the aircraft and a

southern group (S) with a more counterclockwise orientation. As the progression from white lines (position at 1500 UTC) to yellow lines (1515 UTC) shows, the bands were moving quickly south-southeastwards. The aircraft cross section crossed B0, B1 and B2, reaching its northern turn in a gap in the precipitation along the much-larger B3 band which flanks the southern side of the bent-back front.

Figure 8a shows the relative humidity from the aircraft overlain with surface precipitation rate estimated from the radar network (red). The flight leg crossed two cloud bands (RH ≥ 100%), identified as bands B1 and B2 in Fig. 7, which were clearly precipitating at the time of crossing (no cloud was encountered at aircraft altitude during the passage of B0). Note how the wind speed is weaker in the bands than in the clearer air in between (Fig. 8b). The aircraft began its 180^{o} platform turn at 1516 UTC just as it reached B3, rendering its wind measurements unreliable, so the section of flight through B3 is not shown in Fig. 8.

FIgures 8c and 8d show measurements of liquid and ice-number concentrations across the bands, from the Cloud Droplet Probe (CDP) and Cloud Imaging Probe (CIP-100) respectively; details of the microphysics instrumentation are given in Lloyd *et al*. (2014). The clouds contained mixed liquid and ice, with relatively high concentrations of ice particles, images of which show complex aggregates of plate-like crystals (Fig. 9a) as well as high concentrations of columnar crystals at temperatures between -5° and -8°C, characteristic of secondary ice formed by rime splintering (Hallett and Mossop 1974) (Fig. 9b). Substantial ice concentrations were also found in regions sub-saturated with respect to ice. One of the main objectives of DIAMET was to quantify diabatic heating and cooling rates using the observed microphysics, to compare with and improve model simulations. As an example of this, the method described in Dearden et al (2014) has been used to calculate instantaneous diabatic heating and cooling rates associated with the growth and evaporation of ice crystals by vapor diffusion along this section of the flight (Fig 8e). The

calculations made use of relative humidity derived from the WVSS-II hygrometer data, and ice particle size distributions from the CIP-100 probe in the range 0.1 to 6.2 mm (this probe agreed well with other probes in the size range below 1 mm, see Fig 9c). We obtained information on ice particle shapes from the imaging probes and used this to constrain the calculations (red line, Fig 8e). However, many existing bulk microphysics schemes assume fixed shapes for ice crystals to determine the rate of change of ice mass by vapor diffusion, with some simply assuming spherical particles such that the dimension of a particle represents its diameter (e.g. Wilson and Ballard 1999, as used by the Met Office Unified Model; Morrison et al. 2005; Liu et al. 2003). To explore the impact of particle geometry, calculations were also performed assuming the ice particles were spherical during diffusion growth, with a diameter equal to the maximum dimension (blue line, Fig 8e). The results show that for a given particle size distribution, the assumption of spherical shapes leads to an overestimation of the heating and cooling rates by a factor of two or more.

The regions of diabatic heating at 1510–1511 UTC and 1513–1514 UTC both coincide with small decreases in wind speed, consistent with transport of lower-momentum air from below in shallow convective updrafts. The instantaneous cooling rates in the clear air were observed on the southern side of the cloud bands. This raises a question regarding the dynamical mechanism responsible for the emergence of banding in this region of intense cyclones that could explain the relationship between the cloud and wind in such bands, and whether there could be a cooperative feedback from diabatic heating and cooling on the winds (both vertical and horizontal components). We now examine surface wind observations during the passage of the bands.

SURFACE WIND OBSERVATIONS. Figure 10 shows the position of rainbands with time along a straight line joining AWS sites on the islands of Tiree and Islay (Fig. 8). Distance is measured from north-northwest to south-southeast. The precipitation rate at 5-minute intervals estimated by the radar network has been interpolated to the section to create the time–distance progression of

rainfall rate. Wind-gust strength (5-minute running median to be consistent with the radar update interval) is overlain for both AWS sites, after subtracting a 90-minute running median to remove the larger-scale variation. White curves indicate the progression of rainbands along the section, identified using animations of the radar images. Band B1 moved from Tiree (point T) at 1445 UTC to Islay (I) at 1610 UTC and was intercepted by the aircraft at point A (1510 UTC). Note the variability in the precipitation rate of this rainband as it moved along the section; as well as moving south-southeastward, the cloud bands changed morphology noticeably between 5-minute radar images. One rainband appeared to split into two at around 1500 UTC: band B1 moved towards the ESE whereas B2 was more stationary, curving almost parallel to the bent-back front (Fig. 7). The rain reaching Tiree at 1515 UTC (Fig. 7) was at the tip of a much broader precipitation feature advancing rapidly from the west-northwest along the bent-back front, which we do not discuss here. At about 1615 UTC, another precipitation band B4 emerged between band B2 and the bent-back front.

Consistent with the aircraft observations at 840 hPa, the surface wind speed was lower in the core of rainband B1 and immediately after it (at T and I) than in the clear air either side. Similar dips in wind speed occurred during the passage of band B2 across Islay (1715 UTC) and also the earlier bands S1 and S2. To see if this relationship held more generally, data from all 13 AWS sites across central Scotland were examined for this day. The mode of wind speed within the rainbands was 1.5 m s^{-1} lower than between them, while locally the peak-to-trough variation in surface gust strength associated with bands was as much as 10 m s^{-1}. In summary, both at aircraft altitude and at the surface there is evidence that the wind speed tends to dip during the passage of a rainband, and to be higher in the clear air in between. Given the linear nature of the rainbands and their tendency to align along the mean wind, this suggests that the strongest surface winds (and

362 therefore damage) will be arranged in linear swathes. We now examine forecast model predictions of the storm to see how well the Met Office Unified Model simulated these features.

364 **ENSEMBLE PREDICTION OF BANDING IN THE HIGH-WIND REGION.** DIAMET IOP8 provided an ideal test case for the new MOGREPS (Met Office Global and Regional Ensemble Prediction
366 System) convection-permitting forecast system prior to its operational implementation. The MOGREPS-UK ensemble is now run routinely and consists of 12 forecasts run every 6 h with the
368 Met Office Unified Model, on a limited area spanning the UK with a horizontal grid spacing of 2.2 km. For DIAMET IOP8, each ensemble member took its initial and boundary conditions from the
370 corresponding North Atlantic and European regional version of MOGREPS (Bowler et al. 2008). Figure 11 shows a snapshot at 1600 UTC from the first four MOGREPS-UK members, zooming in on
372 Scotland. The color shading is the 850-hPa wind speed, and lines indicate the axes of wind-speed maxima. Figure 12 overlays the same lines on the model precipitation rates. The high-wind cores
374 generally lie along the clear slots between the rainbands. The same is true of the operational deterministic Met Office 1.5-km (UKV) model forecast (not shown). This structure and magnitude
376 of variation is consistent with the *in-situ* aircraft observations presented in Fig. 8.

Each of the 12 ensemble forecasts exhibited banding in precipitation and winds, and we now
378 examine how well the observed precipitation structure was represented and its dependence on length scale (L). Roberts and Lean (2008) and Roberts (2008) introduced a measure of the
380 similarity of a forecast pattern of precipitation rate to the radar-derived rate called the Fractions Skill Score (FSS). First, the radar and forecast data are interpolated onto the same regular grid.
382 Then neighbourhoods are defined as squares of side L and we compute the fraction of pixels within each neighbourhood that have a rain rate exceeding a certain threshold. The calculation is
384 repeated for neighbourhoods centered on every grid box, using both radar and forecast data. If the precipitation fraction in a forecast matches the observed fraction in every neighbourhood

386 square, the FSS equals 1. The lowest possible score for a complete mismatch everywhere is 0, and a score of 0.5 indicates a minimum level of satisfactory spatial agreement (the forecast pattern is
388 in agreement more often than it is not).

Figure 13 shows the FSS versus scale, averaged for Scotland over forecast lead times of 4–24 hours
390 (for a rain rate threshold of 2 mm hr^{-1}). The FSS increases with scale and exceeds 0.5 for scales greater than 25 km for the best ensemble member. The precipitation pattern is highly dependent
392 upon initial conditions, with the worst ensemble member having FSS < 0.5 even for the 110-km scale (associated with a displacement of the cyclone). The precipitation pattern is dominated by
394 the bands which have a characteristic spacing ranging from 20 to 50 km, so the statistics indicate that the model must have captured the positioning of the bands to some extent. Those ensemble
396 members that have a strong match (high FSS) when the bands first emerge maintain the highest FSS throughout the forecast, showing that the model is capable of simulating the evolution of the
398 bands, given favourable initial conditions. Currently, the DIAMET team is evaluating the MOGREPS-UK ensemble performance in precipitation forecasts using FSS, and relating skill in
400 precipitation to the skill in the forecasts of mesoscale features which are associated with precipitation, such as fronts.

402 **CONCLUSIONS.** The second DIAMET campaign took place at a time of exceptionally strong flow across the North Atlantic and vigorous cyclone frequency and intensity over northwestern Europe.
404 The DIAMET flights were the first aircraft missions with comprehensive cloud instrumentation to sample the strong wind region south of a cyclone center. IOP8 took the investigators into the
406 extreme winds of extratropical cyclone Friedhelm, which had a T-bone frontal structure with bent-back front. A phenomenon of particular interest was the cloud and precipitation banding in the
408 strong winds found in the southern quadrant of the storm.

The FAAM aircraft traversed this region between 2000 and 700 m altitude crossing three cloud bands, two of which were precipitating at the time. The clouds were found to be of mixed phase with high number concentrations of secondary ice crystals in the form of columns, consistent with ice multiplication by the Hallett–Mossop (splintering) process. Estimates of the diabatic heating rate were found to be sensitive to the particle shape: assuming spherical ice particles when calculating diffusional growth can lead to errors of a factor of two in the heating rate. Between the bands, sublimating ice particles gave instantaneous diabatic cooling rates of up to 4 K hr^{-1} in a region where (according to dropsonde 4) the atmosphere was close to neutral stability below 800 hPa (2 km).

The horizontal wind speed was lower within the cloud bands than in the clear air between. At 840 hPa, diabatic heating (deduced from the microphysical measurements) occurred where the wind speed decreased, indicating that saturated updrafts were transporting lower-momentum air from the boundary layer below. However, wind measurements from automatic weather stations at the ground also showed a dip in wind speed as rainbands passed overhead. Thus, a link existed between precipitation banding and wind speed throughout the lowest 2 km. Further work is under way to understand the dynamical reasons for the bands and their characteristic spacing.

The DIAMET IOP8 case was one of several used to examine the behaviour of the Met Office MOGREPS-UK 2.2-km ensemble prior to its operational implementation. The forecasts indicated banding in winds and precipitation with the highest wind speeds in the clear slots. The best member matched the structure in precipitation rates observed by radar for length scales of 25 km and above, and this degree of matching was sustained throughout the forecast. This length scale corresponded with the rainband spacing, indicating that the model was capable of forecasting the rainbands and associated wind structures with a positional uncertainty similar to the spacing

between the bands. However, this is only one case, and ensemble forecasts from many cases are required to quantify the skill in probability forecasts of mesoscale features.

Cloud and precipitation banding is often observed in satellite and radar imagery in the southern quadrant of intense extratropical storms. The finding that the precipitation bands are associated with structure in the wind with gusts up to a few m s^{-1} higher in the cloud-free slots, even at the surface, is important for predicting the local impact of cyclonic windstorms. For example, in simple environmental risk models wind damage scales with the third power of wind speed, so even small wind-speed enhancements of several m s^{-1} are potentially important. In IOP8, the rainbands were aligned approximately with the large-scale wind direction, so the highest wind gusts would have been concentrated along linear swathes. This coherent structure of the wind fields is important for nowcasting, as well as for short-range forecasting where there is now potential skill in predicting wind-band structure (even if not the precise location) using high-resolution models.

Acknowledgments. DIAMET is funded by the Natural Environment Research Council (NERC) as part of the Storm Risk Mitigation Programme (NE/I005234/1) in collaboration with the Met Office. The BAe-146 Atmospheric Research Aircraft is flown by Directflight Ltd. and managed by the Facility for Airborne Atmospheric Measurements (FAAM) on behalf of NERC and the Met Office. We particularly thank Captain Alan Foster and Co-Pilot Ian Ramsay-Rae for flying in such extreme conditions and working hard to find an airport that would let us land for refuelling during the storm. Figure 3a was supplied by the Dundee Satellite Receiving Station. PK, JO, and TT received funding from the AXA Research Fund as part of the Seamless Approach to Assessing Model Uncertainties in Climate Projections of Severe European Windstorms (SEAMSEW) project.

Box 1: Educational resources

A research project on storms presents an excellent opportunity for outreach activities, and in DIAMET we collaborated with an award-winning educational consultant, Heather Reid (a former broadcast meteorologist), to develop a package of educational resources for school children related to our key science aims. These included two short professionally-filmed videos on "Forecasting the weather" and "Studying severe storms around the UK," as well as four sets of exercises comprising information for the pupils and activities or worksheets. Topics covered included change of state, latent heat, the electromagnetic spectrum, and using observational data. The videos and worksheets are available on the NCAS project website, http://www.ncas.ac.uk/index.php/en/diamet-schools, and are being actively promoted via project partners like the Royal Meteorological Society, the Institute of Physics, and Education Scotland.

The material is aimed at students aged 12–14 years taking science, in particular physics. The topics were chosen to fit broadly into the secondary-school physics curriculum and provide alternative contexts for the "uses of physics" to the more common examples like X-rays in medical physics or heating solid stearic acid to demonstrate latent heat. This topic choice was deliberate. First, the topics fit neatly with the project's focus on diabatic processes and the use of a research aircraft. Second, all too often weather and climate feature in geography rather than physics at school level; a physics background can be vital to access university teaching of these subjects and, more importantly, to develop the skills usually required for a career in the field.

References

Baker L. H., O. Martínez-Alvarado, J. Methven, and P. Knippertz, 2013: Flying through extratropical cyclone Friedhelm. *Weather,* **68**, 9–11.

Baker, L., Rudd, A., Migliorini, S. and Bannister, R., 2014: Representation of model error in a convective-scale ensemble prediction system. *Nonlinear Processes in Geophysics*, **21**. 19-39.

Bowler, N. E., A. Arribas, K. Mylne, K. B. Robertson and S. E. Beare, 2008: The MOGREPS short-range ensemble prediction system, *Quart. J. Roy. Meteor. Soc.,* **134,** 703-722.

Browning, K., 2004: The sting at the end of the tail: Damaging winds associated with extratropical cyclones. *Quart. J. Roy. Meteorol. Soc.,* **130**, 375–399.

Browning, K. A. and M. Field, 2004: Evidence from Meteosat imagery of the interaction of sting jets with the boundary layer. *Meteorol. Appl*., **11**, 277–289.

Browning, K. A., A. M. Blyth, P. Clark, U. Corsmeier, C. Morcrette, J. Agnew, D. Bamber, C. Barthlott, L. Bennett, K. Beswick, M. Bitter, K. Bozier, B. Brooks, C. Collier, C. Cook, F. Davies, B. Deny, M. Engelhardt, T. Feuerle, R. Forbes, C. Gaffard, M. Gray, R. Hankers, T. Hewison, R. Huckle, N. Kalthoff, S. Khodayar, M. Kohler, S. Kraut, M. Kunz, D. Ladd, J. Lenfant, J. Marsham, J. McGregor, J. Nicol, E. Norton, D. Parker, F. Perry, M. Ramatschi, H. Ricketts, N. Roberts, A. Russell, H. Schulz, E. Slack, G. Vaughan, J. Waight, D. Wareing, R. Watson, A. Webb, A. Wieser, and K. Zink, 2007: The Convective Storm Initiation project. *Bull Amer. Met. Soc*., **88**, 1939–1955.

Carlson, T. N., 1980: Airflow through midlatitude cyclones and the comma cloud pattern. *Mon. Wea. Rev*., **108**, 1498–1509.

498 Chagnon, J., S. L. Gray, and J. Methven, 2013: Diabatic processes modifying potential vorticity in a North Atlantic cyclone. *Quart. J. Roy. Meteorol. Soc.,* **139**, 1270–1282.

500

Clark, P. A., K. A. Browning, and C. Wang, 2005: The sting at the end of the tail: Model diagnostics
502 of fine-scale 3-D structure of the cloud head. *Quart. J. Roy. Meteorol. Soc.,* **131**, 2263–2292.

504 Cook, P. A. and I. A. Renfrew, 2014: Aircraft-based observations of air-sea turbulent fluxes around the British Isles. *Quart. J. Roy. Meteorol. Soc.,* DOI: 10.1002/qj.2345, in press.

506

Dearden, C., P. J. Connolly, T. W. Choularton, G. Lloyd, K. Bower, J. Crosier, and G. Vaughan, 2014:
508 Diabatic heating and cooling rates from in-situ microphysics measurements: A case study of a wintertime UK cold front. *Mon. Wea. Rev*., DOI: 10.1175/MWR-D-14-00048.1, in press.

510

Dee, D. P., S. M. Uppala, A. J. Simmons, P. Berrisford, P. Poli, S. Kobayashi, U. Andrae, M. A.
512 Balmaseda, G. Balsamo, P. Bauer, P. Bechtold, A. C. M. Beljaars, L. van de Berg, J. Bidlot, N. Bormann, C. Delsol, R. Dragani, M. Fuentes, A. J. Geer, L. Haimberger, S. B. Healy, H. Hersbach, E.
514 V. Holm, L. Isaksen, P. Kallberg, M. Koehler, M. Matricardi, A. P. Mcnally, B. M. Monge-sanz, J. -. Morcrette, B. -. Park, C. Peubey, P. de Rosnay, C. Tavolato, J. -. Thepaut, and F. Vitart, 2011: The
516 Era-Interim reanalysis: Configuration and performance of the data assimilation system. *Quart. J. Roy. Meteorol. Soc*., **137**, 553–597.

518

Grønås, S., 1995: The seclusion intensification of the New Year's Day storm 1992. *Tellus*, **47A**, 733-
520 746.

522 Hallet, J., and S. C. Mossop, 1974: Production of secondary ice particles during the riming process. *Nature,* **249,** 26–28.

524

Harrison, D. L., R.W. Scovell, and M. Kitchen, 2009: High-resolution precipitation estimates for
526 hydrological uses. *Proceedings of the ICE - Water Management*, **162**, 125–135.

528 Hoskins, B. J., M. E. McIntyre, and A. W. Robertson, 1985: On the use and significance of isentropic potential vorticity maps. *Quart. J. Roy. Meteor. Soc.,* **111**, 887–946.

530

Liu, H-C., P. K. Wang and R. E. Schlesinger, 2003: A numerical study of cirrus clouds. Part I: Model
532 description. *J. Atmos. Sci*., **60**, 1075-1084.

534 Lloyd, G., C. Dearden., T. W. Choularton., J. Crosier and K. N. Bower, 2014: Microphysics observations of warm, cold and occluded frontal systems during the DIAMET campaign. *Mon. Wea. Rev*., submitted.

538 Martínez-Alvarado, O. and R. S. Plant, 2013: Parameterised diabatic processes in numerical simulations of an extratropical cyclone. *Quart. J. Roy. Meteorol. Soc*., doi: 10.1002/qj.2254, in
540 press.

542 Martínez-Alvarado, O., L. H. Baker, S. L. Gray, J. Methven, and R. S. Plant, 2014: Distinguishing the cold conveyor belt and sting jet air streams in an intense extratropical cyclone. *Mon. Wea. Rev.,*
544 doi:10.1175/MWR-D-13-00348.1, in press.

546 Morrison, H., J. A. Curry and V. I. Khvorostyanov, 2005: A new double-moment microphysics
parameterization for application in cloud and climate models. Part I: Description. *J. Atmos. Sci.*, **62**,
548 1665-1677.

550 Neiman, P. J., and M. A. Shapiro, 1993: The life cycle of an extratropical marine cyclone. Part I:
Frontal-cyclone evolution and thermodynamic air–sea interaction. *Mon. Wea. Rev*., **121**, 2153–
552 2176.

554 Neiman, P. J., M. A. Shapiro and L. S. Fedor, 1993: The life cycle of an extratropical marine cyclone.
Part II: Mesoscale structure and diagnostics. *Mon. Wea. Rev*., **121**, 2177–2199.

556

Norris, J., G. Vaughan and D. M. Schultz, 2014: Precipitation in idealised baroclinic waves. *Mon.*
558 *Wea. Rev.,* doi: 10.1175/MWR-D-13-00343.1, in press.

560 Renfrew, I. A., G. W. K. Moore, J. E. Kristjánsson, H. Ólafsson, S. L. Gray, G. N. Petersen, K. Bovis, P.
R. A. Brown, I. Føre, T. Haine, C. Hay, E. A. Irvine, A. Lawrence, T. Ohigashi, S. Outten, R. S. Pickart,
562 M. Shapiro, D. Sproson, R. Swinbank, A. Woolley, and S. Zhang, 2008: The Greenland Flow
Distortion Experiment. *Bull. Amer. Meteor. Soc.,* **89,** 1307–1324.

564

Roberts, N., 2008: Assessing the spatial and temporal variation in the skill of precipitation
566 forecasts from an NWP model. *Met. Apps.,* **15**, 163–169.

568 Roberts, N., and H. W. Lean, 2008: Scale-selective verification of rainfall accumulations from high-
resolution forecasts of convective events. *Mon Wea. Rev*., **136**, 78–97.

570

Sanders, F., and J. R. Gyakum, 1980: Synoptic-dynamic climatology of the “bomb.” *Mon. Wea. Rev.*, **108**, 1589–1606.

Schultz, D. M., and G. Vaughan, 2011: Occluded fronts and the occlusion process: A fresh look at conventional wisdom. *Bull. Amer. Meteor. Soc.,* **92,** 443–466, ES19–ES20.

Shapiro, M. A., and D. A. Keyser, 1990: Fronts, jet streams and the tropopause. *Extratropical Cyclones, The Erik Palmén Memorial Volume,* C. W. Newton and E. O. Holopainen, Eds., Amer. Meteor. Soc., 167–191.

Smart, D. J., and K. A. Browning, 2013: Attribution of strong winds to a cold conveyor belt and sting jet. *Quart. J. Roy Meteorol. Soc*., doi: 10.1002/qj.2162.

Vaughan, G., 2002: The UK MST radar. *Weather*, **57**, 67–73.

Wilson, D. R., and S. P. Ballard, 1999: A microphysically based precipitation scheme for the UK Meteorological Office Unified Model. *Quart. J. Roy. Meteor. Soc*., **125**, 1607–1636.

Figure Captions

590 **Figure 1.** Evolution of jet-stream strength indicated by the zonal wind at 300 hPa averaged over the North Atlantic. (a) Time series from 1 November to 31 January showing 2011–2012 values in
592 blue from ERA-Interim, with the climatological mean (1979–2010) and standard deviation in black (smoothed with a running 7-day mean). The DIAMET campaign period is marked. The letters refer
594 to the strongest cyclones passing over the UK (see text). (b) Normalised histogram of zonal wind for the DIAMET campaign (red), November 2011 to January 2012 (blue), and Nov–Dec–Jan for the
596 whole ERA-Interim period 1979–2010 (black), estimated from 6-h data using Gaussian kernel smoothing. The area under each curve integrates to 1.

598 **Figure** 2. Met Office surface analysis for 1200 UTC 8 December 2011 (Crown copyright).

Figure 3. (a) Infrared image from the AVHRR instrument on *NOAA-19* at 1235 UTC 8 December
600 2011. (b) Rain rate (mm hr^{-1}) at 1300 UTC estimated by the Met Office radar network (1-km grid spacing). At 1234 UTC, the FAAM aircraft reached the storm center (pink dot). A–D indicate
602 rainbands moving to the east-southeast.

Figure 4. (a) Radar-derived precipitation rate (mm hr^{-1}) at 1800 UTC 8 December 2011 when the
604 cyclone center had crossed to northeast Scotland and the banding to the south was most prominent. (b) Maximum 1-minute gusts at surface stations over central Scotland during 8
606 December 2011, filtered using a 10-minute median. Gust strength (ms^{-1}) is colored by the time of occurrence according to scale in upper left corner of the panel.

608 **Figure 5.** Path of the FAAM aircraft on 8 December 2011 with the track colored according to altitude. Black dots indicate dropsonde launches. The flight took off from Exeter at 1048 UTC,
610 landed for refuelling in Teesside at 1607 UTC, took off again at 1729 UTC, and returned to Exeter

at 2110 UTC. The aircraft was at low levels within the strongest winds at around 1500 UTC and again at 1900 UTC.

Figure 6. (Left panel) Cross sections derived from the ten dropsondes released along the first flight leg from 1130 to 1234 UTC of: left panel, relative humidity with respect to ice (colors) and potential temperature (white contours); right panel, wind speed (ms^{-1}, colors) and wind direction (barbs); the wind barbs use the usual convention for wind strength in knots. Numbers in green denote the order in which sondes were dropped and are placed at the corresponding latitude. *In-situ* measurements from the aircraft, flying at a constant pressure of 390 hPa, are shown in the strip at the top.

Figure 7. Precipitation-radar image for 1515 UTC showing the bands intercepted by the aircraft between 1505 and 1516 UTC (rain rate mm hr^{-1}, colored according to scale at bottom). White lines: bands at 1500 UTC corresponding to the labels in Fig. 8a (B3 from shape of clouds where precipitation is absent). Yellow lines: positions of the bands on the 1515 UTC image, showing the southeastward progression of the bands. The southern bands S1 and S2 were not intercepted by the aircraft. White dots on Tiree and Islay denote positions of automatic weather stations.

Figure 8. Measurements from the FAAM aircraft as it flew northward from Islay to Tiree through the strongest low-level winds. (a) Relative humidity with respect to ice along the flight track, computed using WVSS-II data (shading) and rain rate (red line) derived from the radar network (interpolated to the flight track). (b) Wind speed (m s^{-1}, black; the winds highlighted in yellow correspond to regions where the droplet number concentration exceeds 20 cm-3 or the ice number concentration exceeds 5 L-1), radar altitude (x0.1km, grey dashed), temperature (°C, red) and potential temperature (°C, blue). (c) Droplet number concentration (cm^{-3}), as measured by the Cloud Droplet Probe. (d) Ice particle number concentration (l^{-1}) as measured by the CIP-100 probe. (e) Diabatic heating and cooling rates associated with ice deposition and sublimation of ice

crystals. Red line: mean value calculated over 8 s (~ 1 km) intervals using measured particle sizes and shapes; grey shading: 1 Hz values, indicating the variability; blue line: as red line assuming spherical particles and exponential size distribution. Wind speed is shown again in black and yellow, with an expanded scale

Figure 9. (a) Images of ice crystals captured by the Cloud Particle Imager (CPI) within cloud band B1 (from 1510 – 1511 UTC), showing a mixture of columns and complex plate aggregates; (b) as (a) in the middle of cloud band B2 , revealing the dominance of columnar crystals, with evidence of riming and aggregation; (c) comparison of particle size distributions (number of particles m^{-3} per size bin, normalised to unit width) from the CIP-15 and CIP-100 probes, averaged over 1504–1516 UTC. The CIP-15 has a bin width of 15 μm and a maximum detectable size of 930 μm. The CIP-100 has a bin width of 100 μm and can detect precipitation-sized particles up to 6.2 mm.

Figure 10. A time–distance plot of radar-derived precipitation rate (mm hr^{-1}, colored according to scale at bottom) interpolated from the Met Office radar composite to a line connecting observation sites at Tiree and Islay. Distance increases along the section from north-northwest to south-southeast. Labels T and I identify the passage of rainband B1 over Tiree and Islay, respectively, and point A indicates the crossing of this section by the aircraft. The time series of wind gusts (black lines) measured at both AWS sites is overlain at the corresponding distance along the section. A 90-minute running median has been removed from the winds to emphasise the bands. The white curves indicate the progression of rainbands along the section (Fig. 8).

Figure 11. The 850-hPa wind speed (m s^{-1}, colored according to scale at bottom) from the first four members of the MOGREPS-UK trial forecast at 1600 UTC 8 December 2011, 7 h into the forecast. Dashed lines indicate the axes of the wind maxima.

Figure 12. The rain rate (mm h^{-1}, colored according to scale at bottom) from the first four members of the MOGREPS-UK trial forecast at 1600 UTC 8 December 2011, 7 h into the forecast. Red lines indicate the axes of the wind maxima identified in Fig. 11.

Figure 13. Fractions skill score (FSS) measuring the degree of fit between the rain rate pattern in each forecast and the radar data versus horizontal scale, averaged over forecast lead times 4–24 h. The yellow shading indicates the full range of results from the 12-member ensemble and the members 0, 4 and 5 are also indicated. The best ensemble member has a similar pattern to the radar data (FSS > 0.5) for scales greater than 25 km. FSS is calculated over Scotland (54.6–59.3°N, 8.1°W–0.4°E).

Table 1: Instruments carried on the FAAM aircraft for DIAMET

Measurement	Instrument	Key parameters
Temperature	Platinum resistance thermometer	32 Hz, ±0.3°C
Water Vapor	General Eastern 1011B (-25 - +50°C) Buck CR2 (-60 - +30°C) Spectra Sensors WVSS–II tuneable diode laser	4 Hz, ±0.1 - 1 °C in dew/frost pt 1 Hz, ±0.1 - 0.5°C 0.4 Hz
Winds and turbulence	FAAM 5-hole probe	32 Hz, 0.25 m s^{-1}
Profiles below the aircraft Pressure, temperature, humidity Winds Cloud top	Vaisala AVAPS RD94 dropsondes GPS tracking of dropsonde Leosphere ALS450 backscatter lidar	2 Hz, ±0.4 hPa, ±0.2°C, ±2% RH 4 Hz 5 - 30 s (along-track) , 1.5 m (vertical resolution)
Liquid Water	Johnson-Williams hot wire Nevzorov total water probe	4 Hz, ±0.3 g m^{-3} 8 Hz, ±10%
Cloud and aerosol particles	DMT CIP-15 imaging probe DMT CIP-100 imaging probe DMT CDP scattering probe DMT Cloud, Aerosol and Precipitation Spectrometer with Depolarisation (CAPS-DPOL) SPEC 2D-S shadow probe SPEC CPI V1.5 imaging probe DMT Passive Cavity Aerosol Spectrometer Probe (PCASP)	1 Hz, 15 < D < 930 µm 1 Hz, 100 < D < 6200 µm 10 Hz, 3 < D < 50 µm 1 Hz, 15 < D < 1000 µm 100 Hz, 10 < D < 1280 µm 40 Hz, 5 < D < 1000 µm 1 Hz, 0.6 < D < 50 µm
Chemical species Ozone Carbon Monoxide Greenhouse Gases	TECO 49C UV analyser Aerolaser AL5002 fluorescence Los Gatos Cavity Enhanced Absorption FGGA CO_2 CH_4	10 – 30 s, ±2 ppbv 1 Hz, ±4 ppbv 1 Hz, ±0.17 ppmv 1 Hz, ±1.3 ppbv
Upwelling infrared radiation	Heimann KT-19.82 sensor ARIES Fourier Transform Spectrometer	1 Hz, ±0.3 K brightness temperature 4 Hz, 3 – 18 µm, ±0.2 K brightness temperature

674

676

Table 2 DIAMET and T-NAWDEX Pilot Intensive Observation Periods

IOP	Date	Flight	Duration, hours	Drop sondes	Scientific Objective
IOP1	16-Sep-11	B647	4.67	9	Convective rainband ahead of upper-level trough
IOP2	20-Sep-11	B648 (D)	7.35	15	Mesoscale waves running along trailing cold front – good coverage from Chilbolton
IOP3	23-Sep-11	B650 (D)	7.52	18	Rainband developing in diabatic Rossby wave beneath a warm conveyor belt
IOP4	26-Nov-11	B652	5.12	1	Surface fluxes in cold airstream approaching Scotland from the northwest
IOP5a	28-Nov-11	B654	4.75	15	Dropsonde profile across double front approaching from the Atlantic
IOP5b	29-Nov-11	B655 (D)	7.03	13	Intense cold front crossing UK from the west, giving rise to tornadoes on landfall
IOP6	01-Dec-11	B656	5.40	10	Small-scale cyclone Zafer near Shetland; measuring surface fluxes in high winds
IOP7	05-Dec-11	B657	3.13	0	Organised convection west of Scotland
IOP8	08-Dec-11	B658 (D)	9.00	21	Severe winter cyclone Friedhelm; Sting jet case
IOP9	12-Dec-11	B662	4.83	17	Warm front approaching from the west, bringing South coast gales and rainfall
IOP10	30-Apr-12				Slow moving cyclone bringing floods; overnight observations from Chilbolton radar
IOP11a	09-May-12	B694	4.60	8	Warm front of a frontal wave cyclone approaching from the southwest
IOP11b	10-May-12	B695	5.15	19	Warm front of same frontal cyclone over Scotland plus surface fluxes
IOP12	10-Jul-12	B712	4.27	9	Convective rainbands north of a mesoscale PV anomaly
IOP13	18-Jul-12	B715	4.60	11	Stationary warm conveyor belt over Scotland, bringing flooding
IOP14	15-Aug-12	B728	4.50	8	Bent-back front of strong summer cyclone over Ireland
TNP1	03-Nov-09	B483	4.65	11	Cold front capped by tropopause fold. Later developed tornadoes across S. England
TNP2	13-Nov-09	B486	4.70	17	Warm front at leading edge of frontal wave cyclone
TNP3	24-Nov-09	B488	5.23	7	Circuit around surface cold front over ocean and survey of warm conveyor belt

678 Note: flights marked (D) were double flights where the aircraft landed for refuelling mid-mission.

Figures

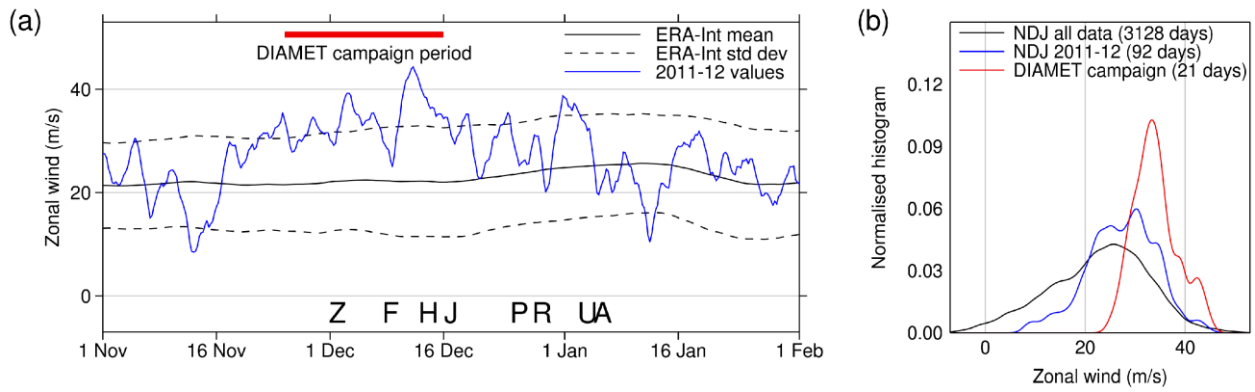

Figure 1. Evolution of jet-stream strength indicated by the zonal wind at 300 hPa averaged over the North Atlantic. (a) Time series from 1 November to 31 January showing 2011–2012 values in blue from ERA-Interim, with the climatological mean (1979–2010) and standard deviation in black (smoothed with a running 7-day mean). The DIAMET campaign period is marked. The letters refer to the strongest cyclones passing over the UK (see text). (b) Normalised histogram of zonal wind for the DIAMET campaign (red), November 2011 to January 2012 (blue), and Nov–Dec–Jan for the whole ERA-Interim period 1979–2010 (black), estimated from 6-h data using Gaussian kernel smoothing. The area under each curve integrates to 1.

694

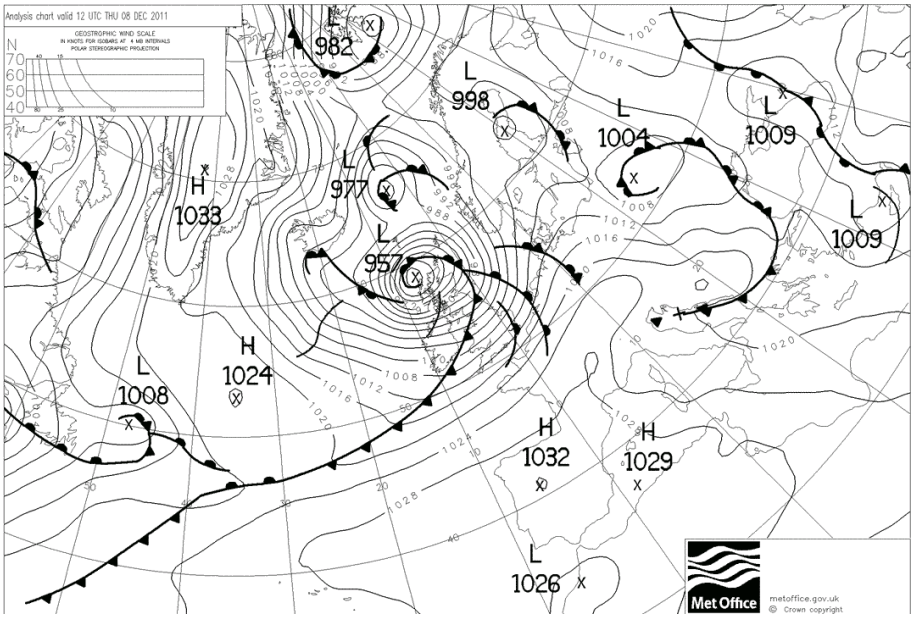

696 Figure 2. Met Office surface analysis for 1200 UTC 8 December 2011 (Crown copyright).

698

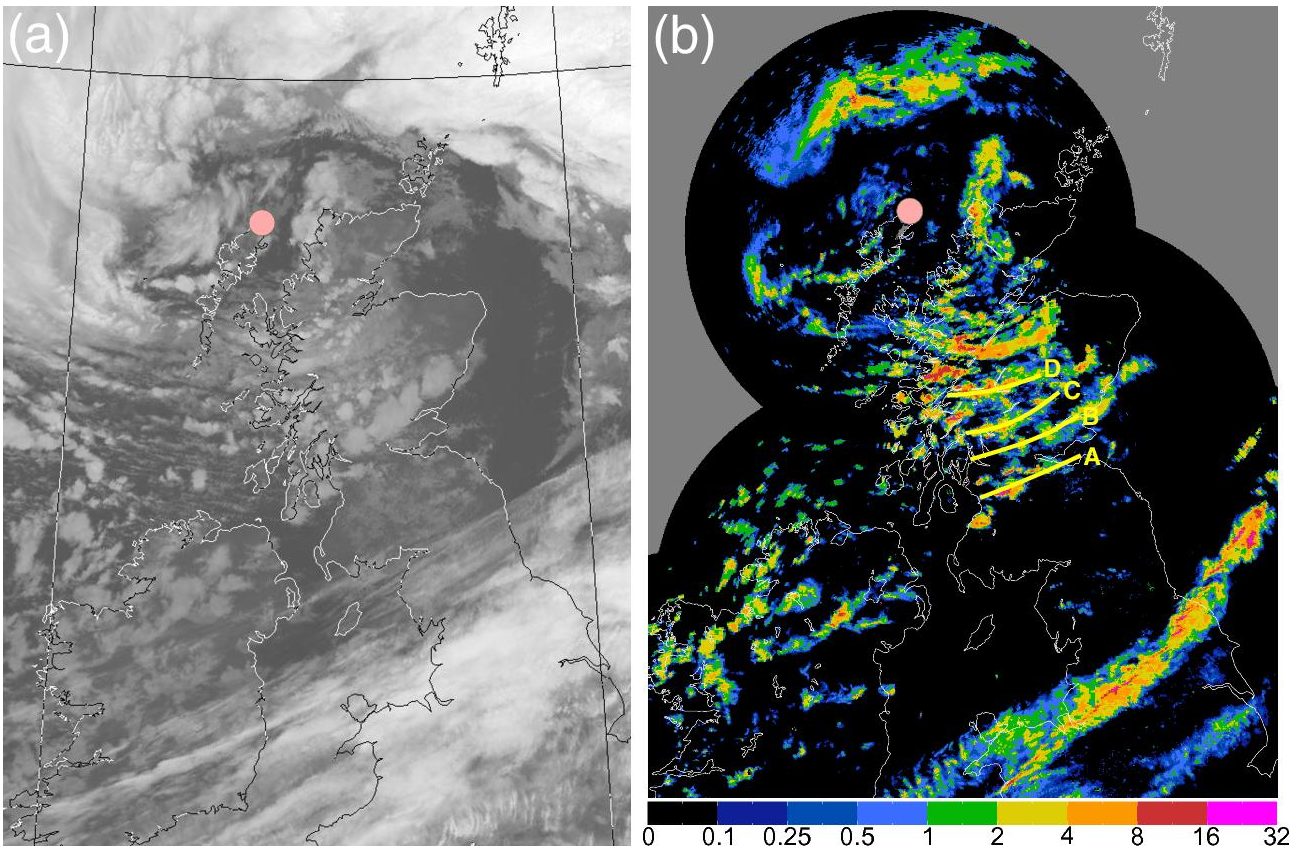

700

Figure 3. (a) Infrared image from the AVHRR instrument on *NOAA-19* at 1235 UTC 8 December
702 2011. (b) Rain rate (mm hr^{-1}) at 1300 UTC estimated by the Met Office radar network (1-km grid spacing). At 1234 UTC, the FAAM aircraft reached the storm center (pink dot). A–D indicate
704 rainbands moving to the east-southeast.

706

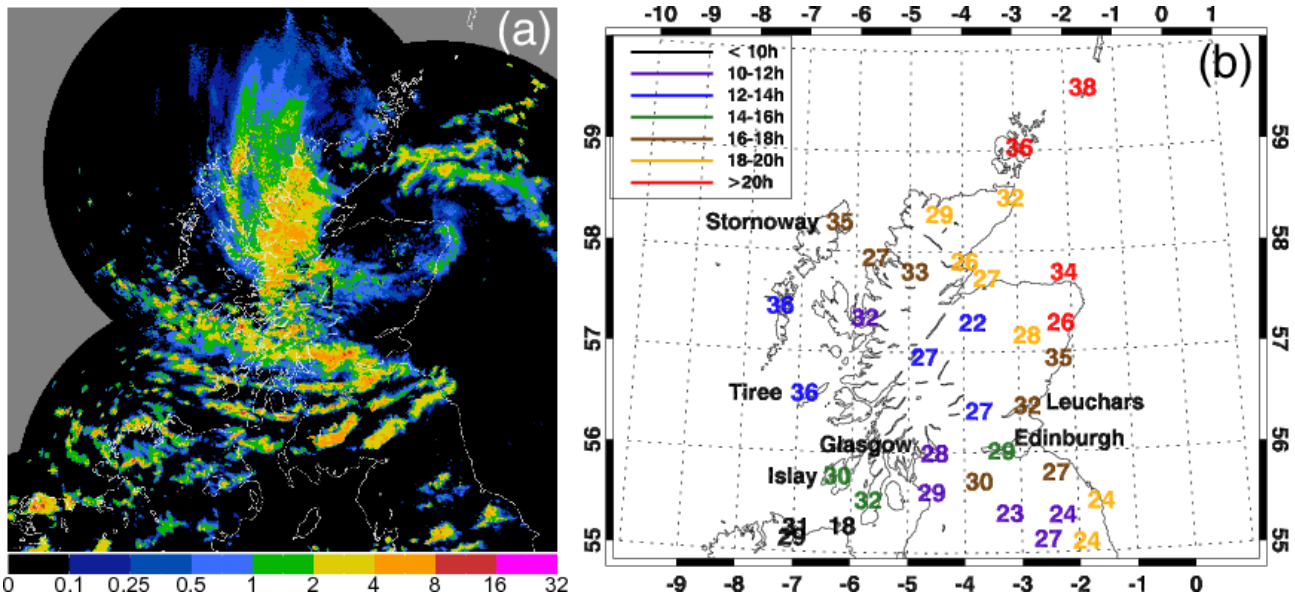

708

710 Figure 4. (a) Radar-derived precipitation rate (mm hr^{-1}) at 1800 UTC 8 December 2011 when the cyclone center had crossed to northeast Scotland and the banding to the south was most
712 prominent. (b) Maximum 1-minute gusts at surface stations over central Scotland during 8 December 2011, filtered using a 10-minute median. Gust strength (ms^{-1}) is colored by the time of
714 occurrence according to scale in upper left corner of the panel.

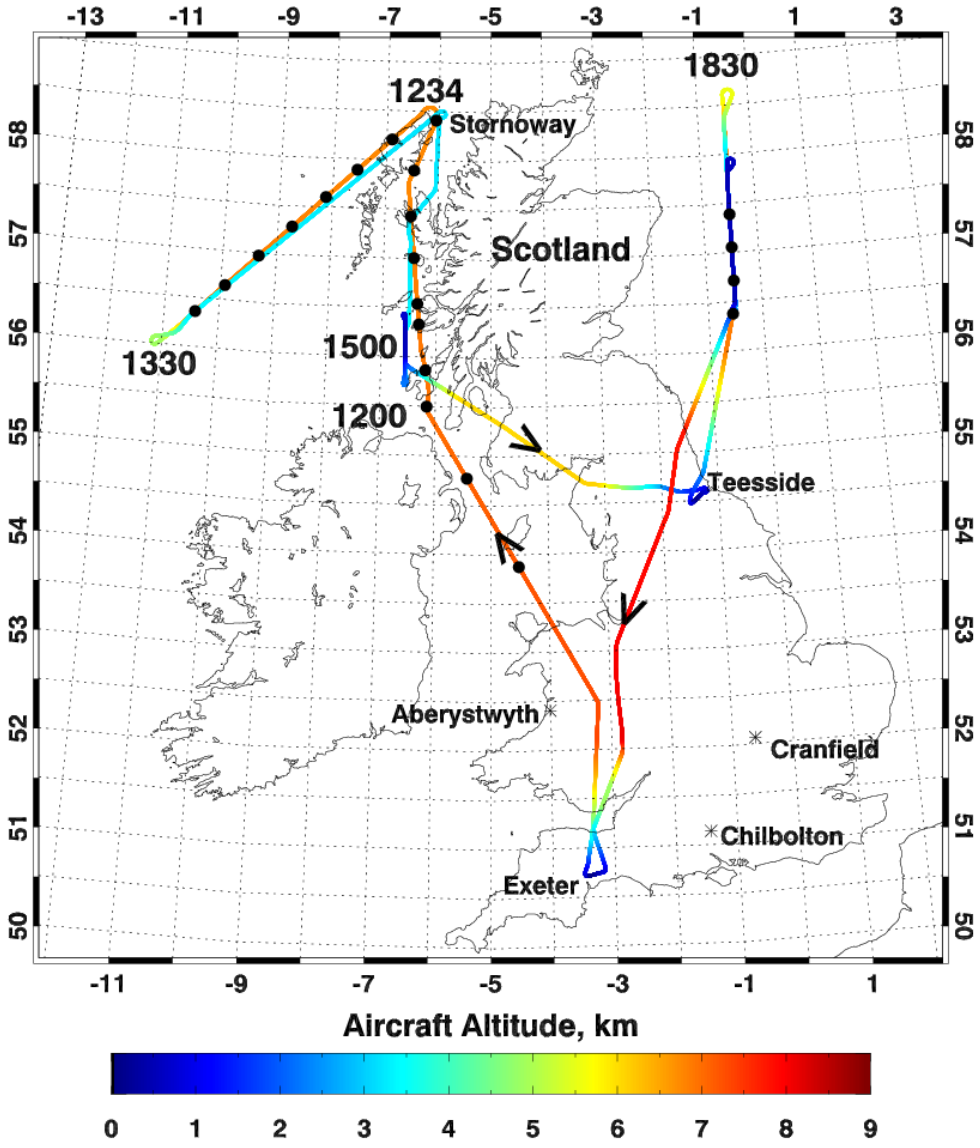

716

Figure 5. Path of the FAAM aircraft on 8 December 2011 with the track colored according to
718 altitude. Black dots indicate dropsonde launches. The flight took off from Exeter at 1048 UTC, landed for refuelling in Teesside at 1607 UTC, took off again at 1729 UTC, and returned to Exeter
720 at 2110 UTC. The aircraft was at low levels within the strongest winds at around 1500 UTC and again at 1900 UTC.

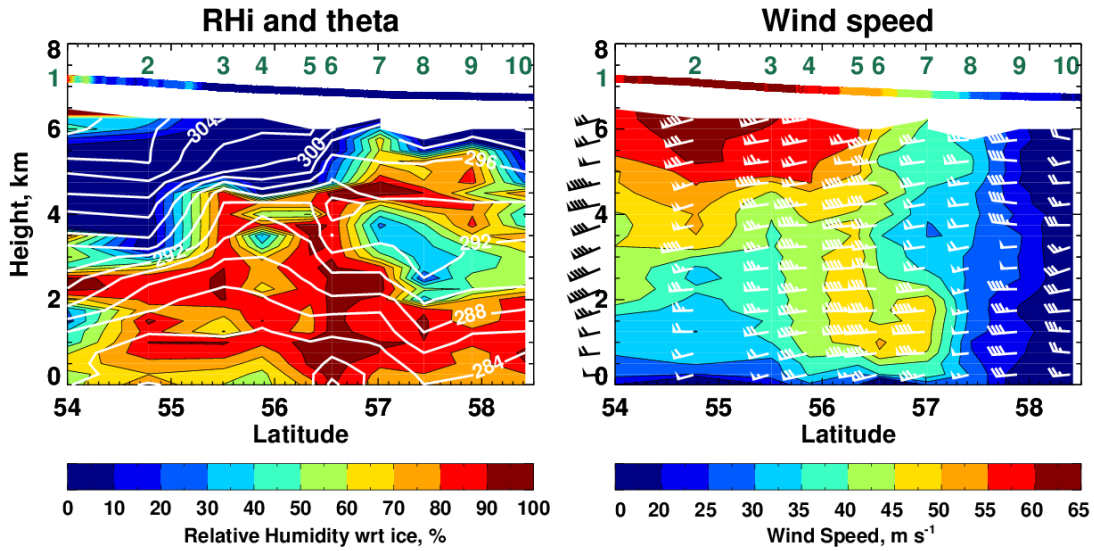

722

Figure 6. (Left panel) Cross sections derived from the ten dropsondes released along the first flight
724 leg from 1130 to 1234 UTC of: left panel, relative humidity with respect to ice (colors) and potential temperature (white contours); right panel, wind speed (ms^{-1}, colors) and wind direction
726 (barbs); the wind barbs use the usual convention for wind strength in knots. Numbers in green denote the order in which sondes were dropped and are placed at the corresponding latitude. *In-*
728 *situ* measurements from the aircraft, flying at a constant pressure of 390 hPa, are shown in the strip at the top.

730

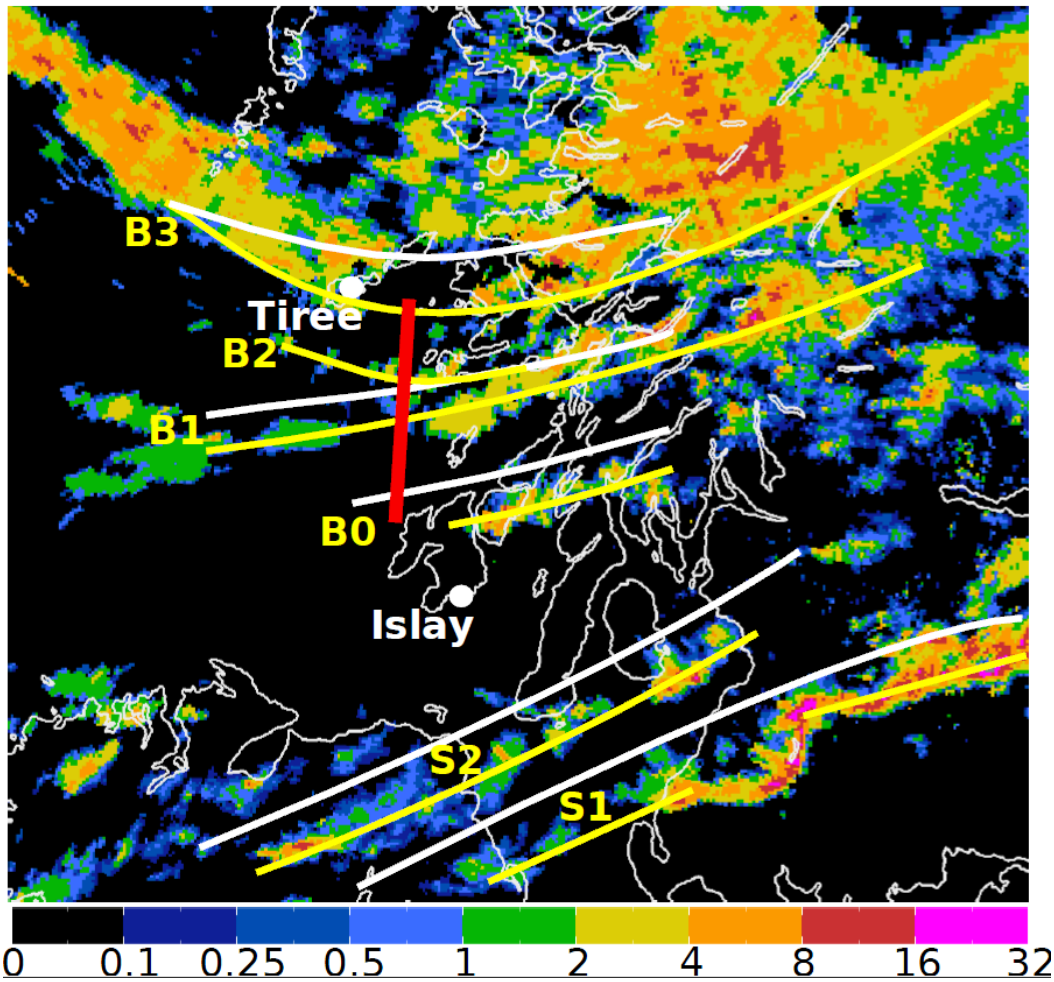

732

Figure 7. Precipitation-radar image for 1515 UTC showing the bands intercepted by the aircraft
734 (red track) between 1505 and 1517 UTC (rain rate mm hr^{-1}, colored according to scale at bottom). White lines: bands at 1500 UTC corresponding to the labels in Fig. 8a (B3 from shape of clouds
736 where precipitation is absent). Yellow lines: positions of the bands on the 1515 UTC image, showing the southeastward progression of the bands. The southern bands S1 and S2 were not
738 intercepted by the aircraft. White dots on Tiree and Islay denote positions of automatic weather stations.

740

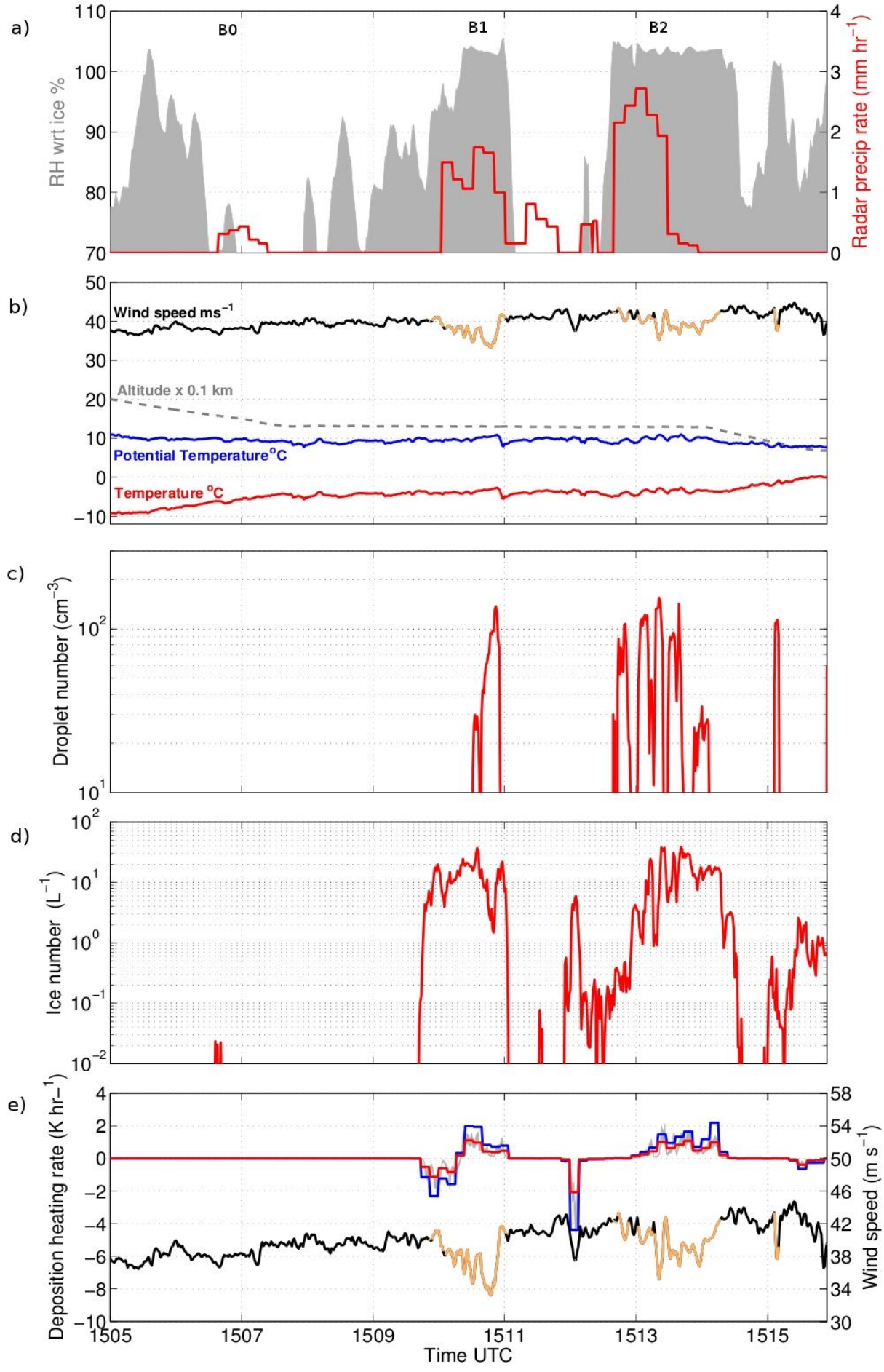

742 Figure 8. Measurements from the FAAM aircraft as it flew northward from Islay to Tiree through

744 the strongest low-level winds. (a) Relative humidity with respect to ice along the flight track, computed using WVSS-II data (shading) and rain rate (red line) derived from the radar network
746 (interpolated to the flight track). (b) Wind speed (m s^{-1}, black; the winds highlighted in yellow correspond to regions where the droplet number concentration exceeds 20 cm^{-3} or the ice
748 number concentration exceeds 5 l^{-1}), radar altitude (x0.1km, grey dashed), temperature (°C, red) and potential temperature (°C, blue). (c) Droplet number concentration (cm^{-3}), as measured by
750 the Cloud Droplet Probe. (d) Ice particle number concentration (l^{-1}) as measured by the CIP-100 probe. (e) Diabatic heating and cooling rates associated with ice deposition and sublimation of ice
752 crystals. Red line: mean value calculated over 8 s (~ 1 km) intervals using measured particle sizes and shapes; grey shading: 1 Hz values, indicating the variability; blue line: as red line assuming
754 spherical particles and exponential size distribution. Wind speed is shown again in black and yellow, with an expanded scale

756

758

760

a)

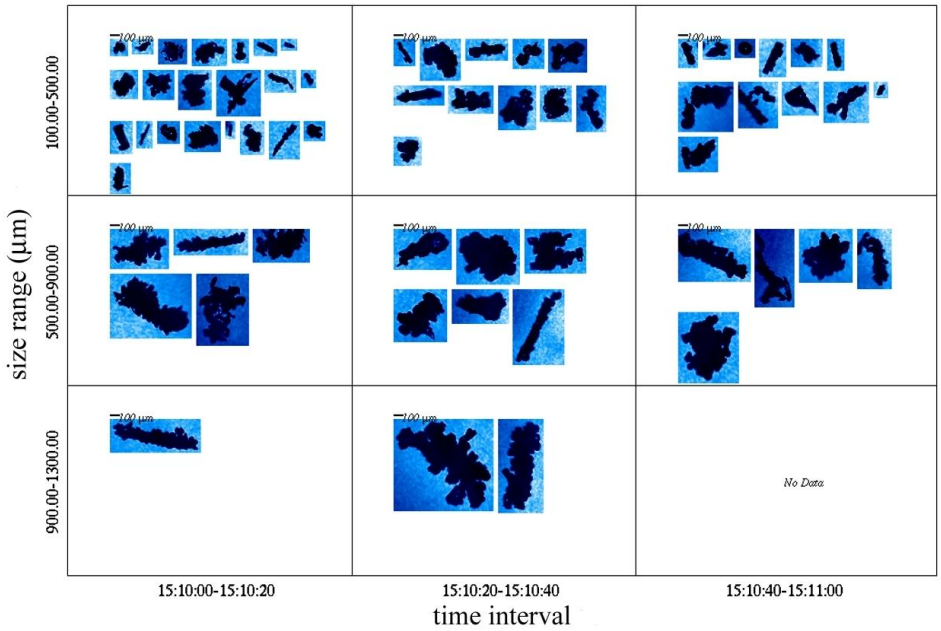
100 µm
100.00-500.00
500.00-900.00
900.00-1300.00
size range (µm)
No Data
15:10:00-15:10:20
15:10:20-15:10:40
15:10:40-15:11:00
time interval

b)

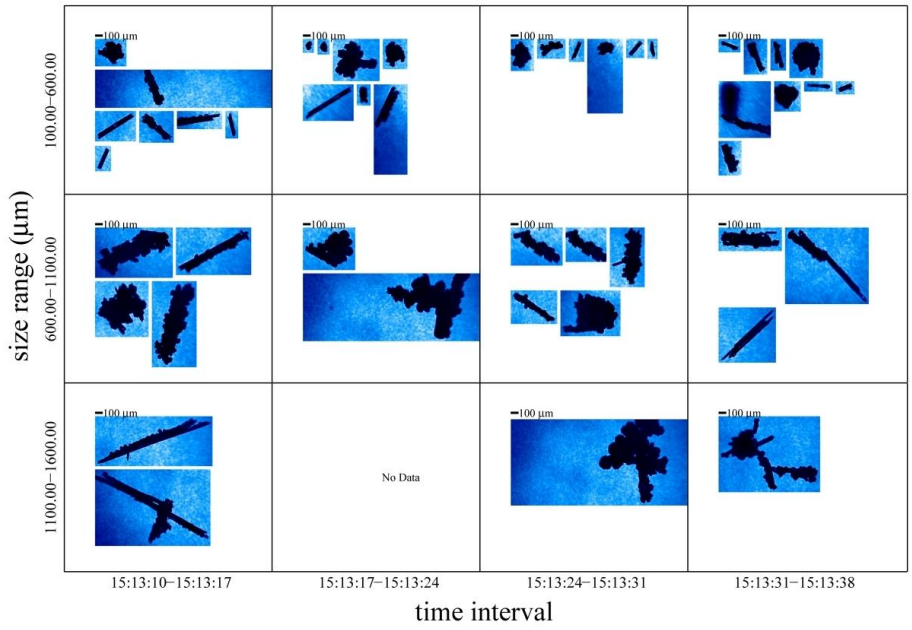
100 µm
100.00–600.00
600.00–1100.00
1100.00–1600.00
size range (µm)
No Data
15:13:10–15:13:17
15:13:17–15:13:24
15:13:24–15:13:31
15:13:31–15:13:38
time interval

c)

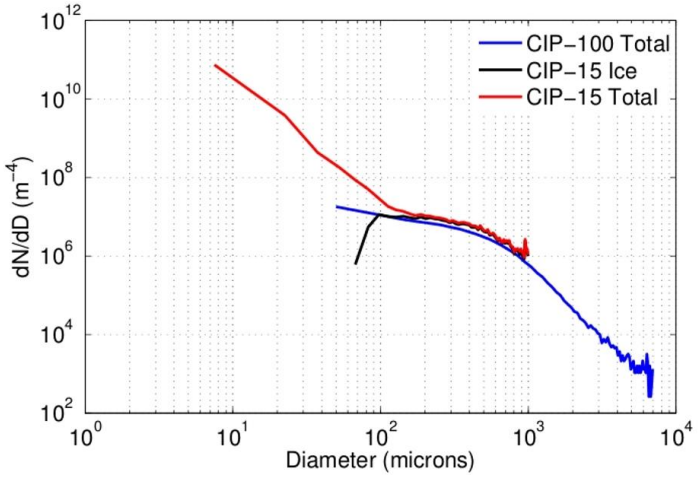
CIP–100 Total
CIP–15 Ice
CIP–15 Total
dN/dD (m^{-4})
Diameter (microns)

762

Figure 9. (a) Images of ice crystals captured by the Cloud Particle Imager (CPI) within cloud band B1 (from 1510 – 1511 UTC), showing a mixture of columns and complex plate aggregates; (b) as (a) in the middle of cloud band B2, revealing the dominance of columnar crystals, with evidence of riming and aggregation; (c) comparison of particle size distributions (number of particles m^{-3} per size bin, normalised to unit width) from the CIP-15 and CIP-100 probes, averaged over 1504–1516 UTC. The CIP-15 has a bin width of 15 µm and a maximum detectable size of 930 µm. The CIP-100 has a bin width of 100 µm and can detect precipitation-sized particles up to 6.2 mm.

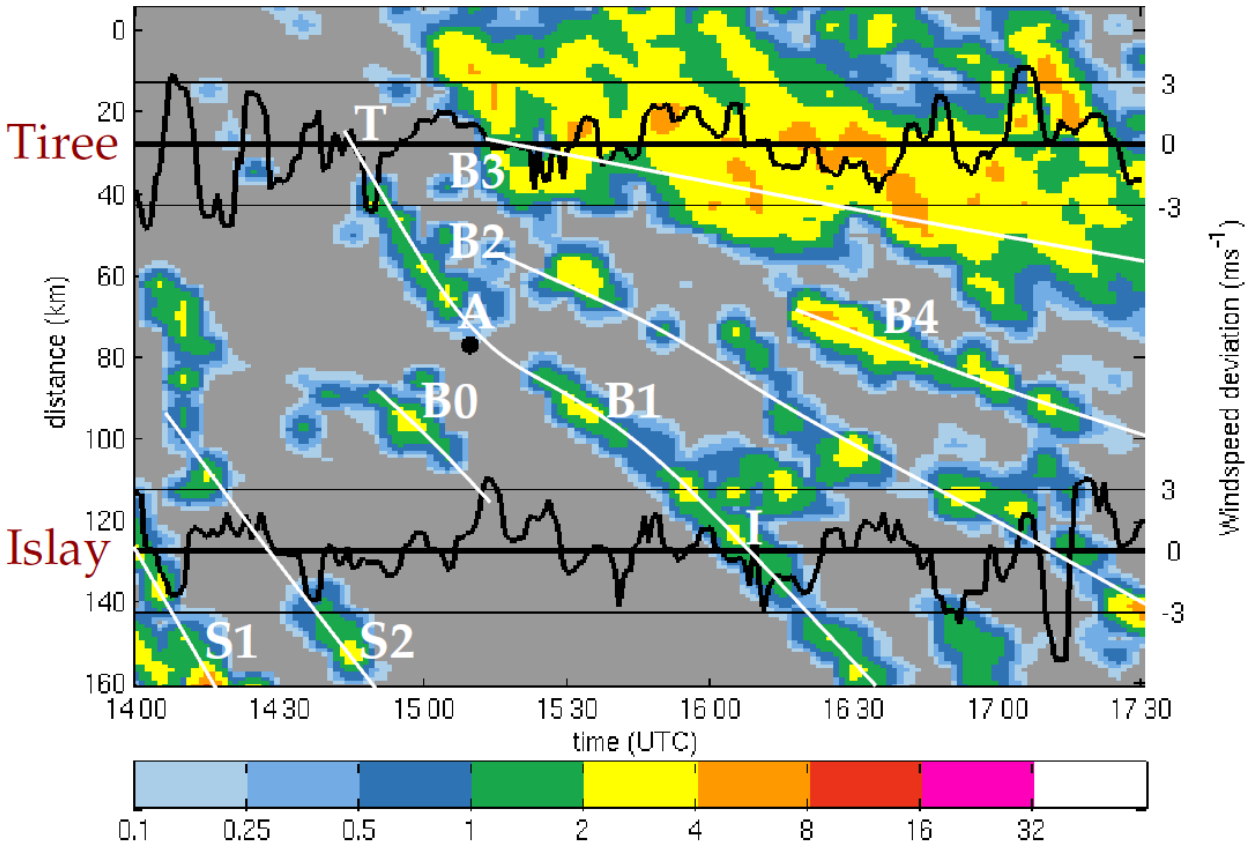

Figure 10. A time–distance plot of radar-derived precipitation rate (mm hr^{-1}, colored according to scale at bottom) interpolated from the Met Office radar composite to a line connecting observation sites at Tiree and Islay. Distance increases along the section from north-northwest to south-southeast. Labels T and I identify the passage of rainband B1 over Tiree and Islay, respectively, and point A indicates the crossing of this section by the aircraft. The time series of wind gusts (black lines) measured at both AWS sites is overlain at the corresponding distance along the section. A 90-minute running median has been removed from the winds to emphasise the bands. The white curves indicate the progression of rainbands along the section (Fig. 8).

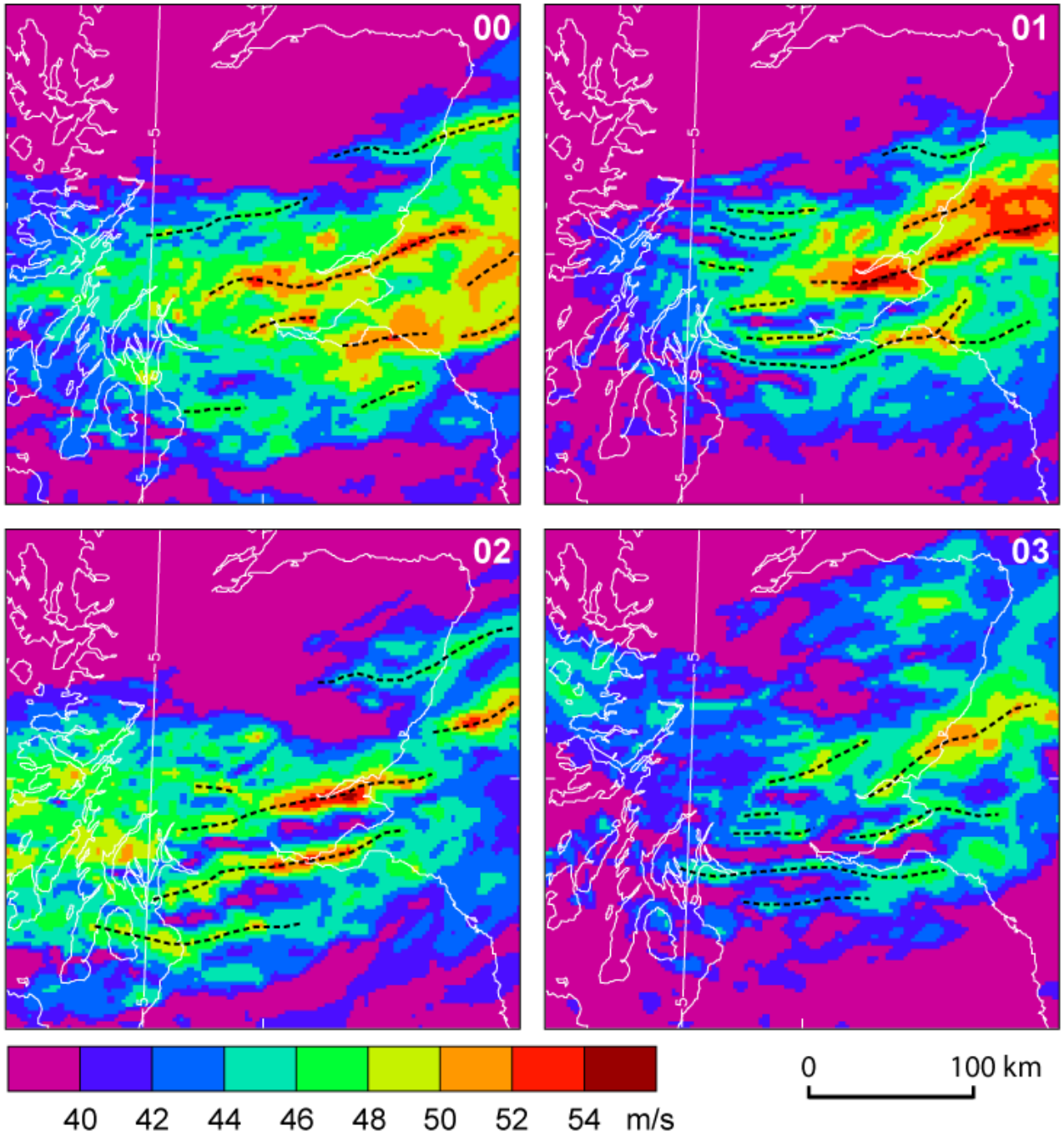

Figure 11. The 850-hPa wind speed (m s^{-1}, colored according to scale at bottom) from the first four members of the MOGREPS-UK trial forecast at 1600 UTC 8 December 2011, 7 h into the forecast. Dashed lines indicate the axes of the wind maxima.

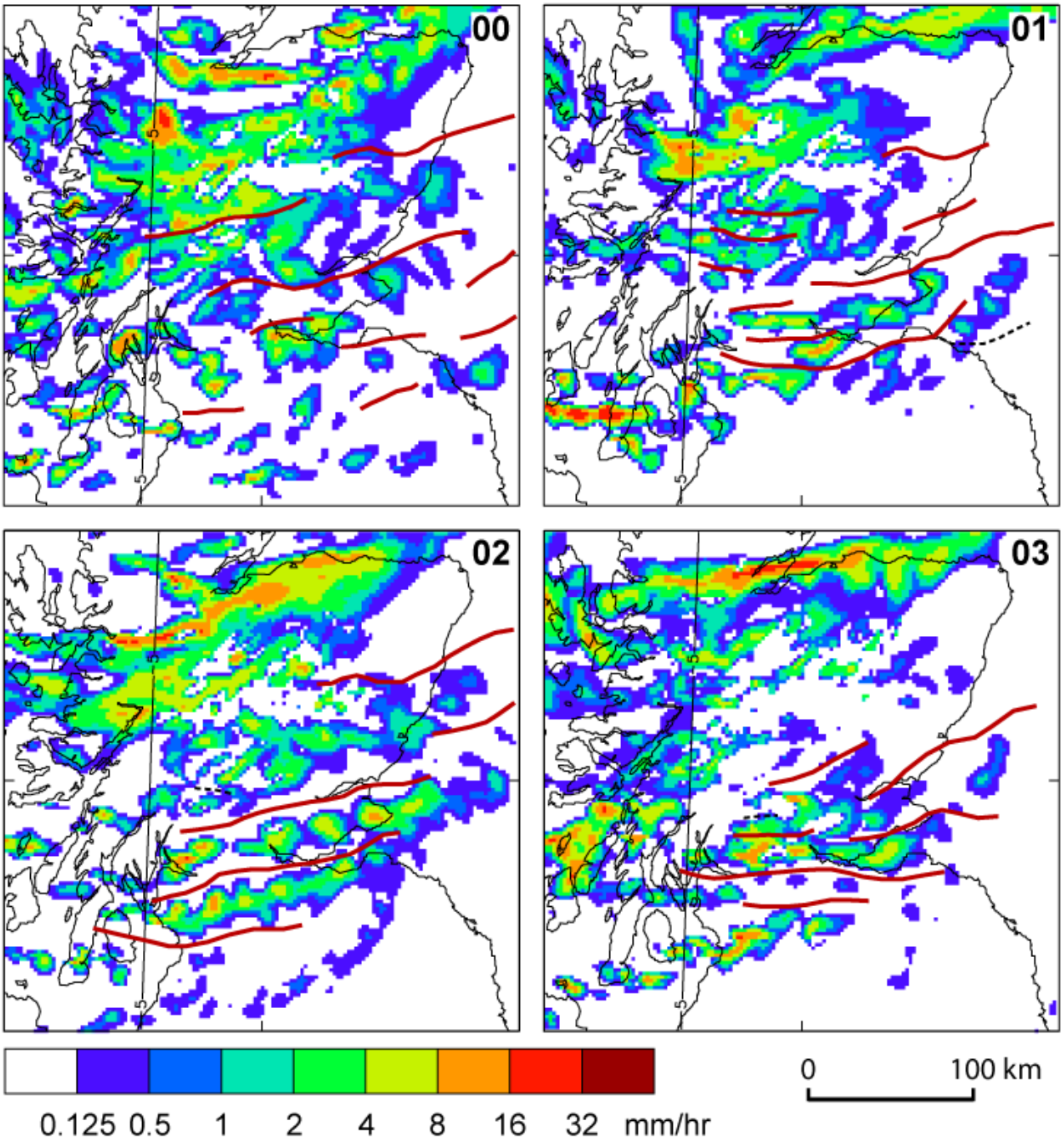

792 Figure 12. The rain rate (mm h^{-1}, colored according to scale at bottom) from the first four
members of the MOGREPS-UK trial forecast at 1600 UTC 8 December 2011, 7 h into the forecast.
794 Red lines indicate the axes of the wind maxima identified in Fig. 11.

796

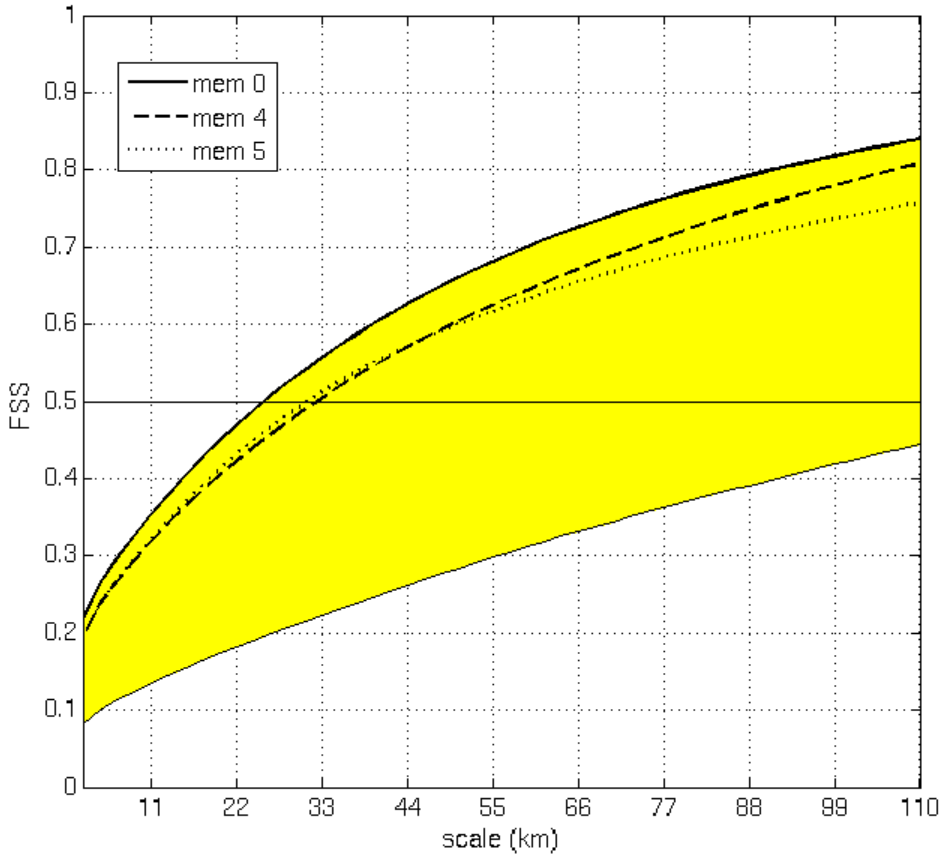

Figure 13. Fractions skill score (FSS) measuring the degree of fit between the rain rate pattern in each forecast and the radar data versus horizontal scale, averaged over forecast lead times 4–24 h. The yellow shading indicates the full range of results from the 12-member ensemble and the members 0, 4 and 5 are also indicated. The best ensemble member has a similar pattern to the radar data (FSS > 0.5) for scales greater than 25 km. FSS is calculated over Scotland (54.6–59.3°N, 8.1°W–0.4°E).